Mine Water and the Environment (2018) 37:272–280
https://doi.org/10.1007/s10230-018-0529-x

TECHNICAL ARTICLE

Experimental Study of a Tailings Impoundment Dam Failure Due to Overtopping

Teng Wu[1] · **Jie Qin**[1]

Received: 27 January 2017 / Accepted: 12 March 2018 / Published online: 15 March 2018

Abstract
The disastrous impact of a tailings dam failure is more far-reaching than that of a water retention dam failure. This paper analyzes the movement characteristics of mudflow during a tailings dam failure using physical models based on the Wadugou tailings impoundment. The physical models were built according to the similarity laws to investigate an overtopping dam failure under natural conditions and when additional protective measures were used. Based on the experimental results, the dam breach size, the breach flow discharge, flow velocity, downstream inundated area, and tailings deposition volume are all reduced by preferably protecting and maintaining the tailings dam embankment to mitigate the destructive effects of a potential dam failure. Finally, the time required for safe evacuation for the Wadugou tailings impoundment area is given.

Keywords Dam break · Tailings pond · Physical model · Model scale

Introduction

Tailings dams are built to store waste from mining activities. Currently, China has more than 12,000 tailings impoundments and nearly 95% of them discharge tailings directly at the dam crest as the embankment dams are raised progressively to the design height (Yin et al. 2008). Each year, about 200 new tailings impoundments are constructed in China, and the failure of tailings dams has become a major problem (Yin et al. 2011). A number of particular characteristics make tailings dams more vulnerable to failure than water retention dams. Failure of a tailings dam may result from a variety of causal mechanisms (e.g. flooding, piping, overtopping, liquefaction, or a combination of these), and spill out a large amount of polluted water and tailings (Rico et al. 2008).

Floods caused by a tailings dam failure is a serious issue faced by many countries (Costa and Schuster 1988; Miller and Cruden 2002; Nicoletti and Parise 2002; Korup and Tweed 2007; Rico et al. 2008). In 1985, a tailings dam of the Prestavel fluorite mine, near Tesero (Trento), Northern Italy, failed, causing a disastrous mudflow, which completely destroyed most of the buildings standing along the stream in Tesero and caused 268 deaths (Sammarco 2004). Another widely known tailings dam disaster is the Los Frailes (Aznalcollar) accident that occurred in April 1998; about 147 million euro was spent to correct the negative environmental and agricultural impacts (Riba et al. 2006; Rico et al. 2008). In China, failures of tailings dams have resulted in tremendous losses of life and property, and serious risks to the environment. For example, on 10 August 2008, a dam failure at an iron ore tailings impoundment in Shanxi province, China, caused 277 deaths (Yin et al. 2011).

A valid emergency plan for a potential tailings dam failure is supposed to provide an early warning of a potential failure and instruct possibly-threatened residents to evacuate. The timeliness of an early warning directly influences the post-disaster survival rate of the downstream residents. Statistics indicate that if the warning is issued 90 min in advance, the mortality rate of downstream residents may be only 0.02%. However, if the warning is issued less than 15 min in advance, the mortality rate rises to 50% (Simpson and Castelltort 2006; Wang et al. 2011; Yin et al. 2011). Therefore, it is necessary to predict the process of a potential tailings dam failure, specifically the characteristics of hydrograph of a flood caused by the dam failure.

Simple estimations can be performed based on empirical relations that relate key dam failure hydrological parameters to pre-failure physical characteristics based on information

✉ Jie Qin
jqin@hhu.edu.cn

[1] College of Harbour, Coastal and Offshore Engineering, Hohai University, Nanjing, China

from reported dam failures. The hydrological parameters usually include outflow volume, peak discharge, and tailings moving distance. For tailings dams, the usefulness of empirical relationships is limited because of the scarcity of reliable historical data. In addition, these empirical relationships require detailed geotechnical data of the tailings as well as the geometry of the downstream valley, which is not always available (Rico et al. 2008).

In addition to the pre-mentioned shortcomings, the empirical relations cannot simulate the dam failure process. The dam failure process can be simulated by numerical or physical models (Jeyapalan et al. 1983; Yin et al. 2011). These models provide an important basis for the compilation of the emergency plan of tailings dam failure, the site selection of tailings pond, evacuation plans for downstream residents, and the construction and design of downstream buildings (Zhang et al. 2011).

Most such studies simulated tailings dam failures using numerical water retention models in combination with empirical relationships of sediment movement. A significant difference of dam-break incidents between water retention and tailings dams lies in the high sediment concentration of the tailings flow (Rico et al. 2008). Numerical studies conducted by Jeyapalan et al. (1983) investigated several tailings dam failures, and used a Bingham plastic model to account for the high sediment concentration. A more general bibliography about mudflows using the Bingham's model reveals a viscosity range between 30 and 1000 Pa s and a stress threshold range between 0.1 and 12 kPa (De Blasio et al. 2004; Pastor et al. 2007). The viscosity and stress threshold cannot be defined more precisely because of the varied nature of the tailings materials and water content (Prime et al. 2014). Thus, more needs to be done to establish a reliable general methodology for such numerical models.

As an alternative to numerical models, physical models have been used in the field of engineering applications, from ship collision problems (Tabri et al. 2008) to dam failure simulations (Sun et al. 2012). A physical model is a copy of an original object (prototype) scaled down by a certain percentage. Both flow and sediment condition (e.g. the boundary conditions, the flow field, the sediment grain size, and the sediment movement) must be scaled appropriately (Yin et al. 2011). Physical hydraulic models are commonly used during to optimize the design and operation of a hydraulic structure. In a physical model, the flow conditions are said to be similar to those in the prototype if the model displays similarity of form (geometric similarity), similarity of motion (kinematic similarity), and similarity of forces (dynamic similarity) (Chanson 1999).

Most studies of tailings dam failures have focused on the relationship between dam stability and the seepage field of tailings dams; only a few have investigated the overtopping of tailings dams (Yin et al. 2008, 2011; Zandarín et al. 2009; Zhang et al. 2011), although in China, overtopping is the primary cause for 52% of tailings dam failures (Loukola et al. 1993). Measures used to prevent disasters caused by this type of dam failure have mainly focused on two aspects: (1) improving the drainage system, such as spillways, tunnels, and flood interception ditches; and (2) establishing a flood warning system to forecast flood processes (Niekerk and Viljoen 2005). However, if the drainage system does not work normally, the flow will erode the dam body, and the risk of a dam failure increases rapidly. Therefore, if the stability of the dam body itself can be improved to reduce the risk of a dam failure, this would potentially have important practical significance. Zhao et al. (2015) proposed a measure to enhance the stability of the dam body by adding reinforcing bars to the dam. This method, however, is impractical to implement at most sites because the length of the reinforcement bars is close to the width of the dam. This study evaluates a different approach that increases the stability of the dam body by applying a surface protective measure to the dam body, which is inexpensive and relatively easy to construct.

In this paper, the processes of overtopping tailings dam failures were analyzed using the physical model method. The model was built based on similarity laws and used the Wadugou tailings impoundment as a prototype.

Methods

Introduction to the Wadugou Tailings Pond

The Wadugou tailings impoundment is located in Sichuan Province, China. The body of the base dam consists of local rock-fill materials and is 20 m high. The tailings dam was constructed on the base dam with tailings and dirt and was raised to 146 m high through three phases of construction. Both the upstream and downstream gradients of the dam embankments were the same (1:2) during construction. In the first construction phase, the dam crest was 2410 m high, and the dam height was 92 m. The dam crest was 10 m wide and 508 m long. The structural volume of the dam body was about 3.75 million m^3. In the second construction phase, the dam crest was increased to 2440 m high, 10 m wide, and 618 m long. The structural volume of the dam body was about 4.98 million m^3. In the last construction phase, the altitude was further increased to 2460 m, and the dam height reached 146 m. The total storage capacity reaches 24.19 million m^3 and the effective storage capacity reaches 18.14 million m^3 which can meet the 23.9-year production requirement.

Physical Model Scales

As the mechanism of a tailings dam failure is very complicated, it is important to focus on the key issues. One of these key issues is the dynamic similarity of the tailings model, which reflects the similarity of forces between the model and prototype. The major forces in a tailings dam relate to the tailings particles: inertia force, friction, adhesive force, gravity, and elastic force. In most cases, the elastic and adhesive forces are so small that they can be ignored. As a consequence, the inertial force, friction, and gravity are the main forces considered in this study. The similitudes of a tailings dam failure include: the similarity conditions of water-flow gravity: $\lambda_V = {\lambda_H}^{1/2}$; the similarity conditions of water-flow resistance: $\lambda_n = \frac{1}{\lambda_V}\lambda_H^{2/3}\left(\frac{\lambda_H}{\lambda_L}\right)^{1/2}$; the similarity conditions of the tailings sediment carrying capacity: $\lambda_s = \lambda_{s*} = k\frac{\lambda_{\gamma_s}}{\lambda_{(\gamma_s-\gamma)/\gamma}}\frac{\lambda_V}{\lambda_\omega}\left(\frac{\lambda_H}{\lambda_L}\right)^{3/2}$; the similarity conditions of tailings suspension: $\lambda_\omega = \lambda_V\frac{\lambda_H}{\lambda_L}$; the similarity conditions of riverbed deformation: $\lambda_{t2} = \lambda_{t1}\frac{\lambda_{\gamma_0}}{\lambda_s} = \frac{\lambda_{\gamma_0}}{\lambda_s}\frac{\lambda_L}{\lambda_V}$; and the similarity of incipient motion of tailings: $\lambda_{v_c} = \lambda_V$.

In these equations, $k = 1.85$ is a constant that is determined based on a calibration process; λ_L is the horizontal scale; λ_H is the vertical scale; λ_V is the scale of water-flow velocity; λ_n is the scale of roughness coefficient; λ_ω is the scale of settling velocity of tailings sediment; λ_s is the scale of tailings sediment concentration of water flow; λ_{s*} is the scale of tailings sediment-carrying capacity of water flow (Zhang et al. 2007); λ_{t1} is the scale of movement time of water flow; λ_{t2} is the scale of the time of riverbed scouring and silting deformation; λ_{γ_s} is the density scale sediment; λ_{γ_0} is the scale of the dry bulk density of sediment; and λ_{v_c} is the scale of incipient velocity of tailings. Because of the three dimensional characteristics of water flow during the dam failure, an undistorted model is used in this study. For an undistorted model: $\lambda_L = \lambda_H$ and $\lambda_n = \lambda_H^{1/6}$.

The simulated region is a mountainous area and the elevation difference between upstream and downstream is 460 m. To ensure water flow similarity conditions, the water depth of the model must exceed 0.015 m, and the Reynolds number should exceed 2000. Considering these factors, the horizontal and vertical scale of the model were chosen as 180. Another important scale that had to be determined separately was grain size scale, which is defined according to the similitude of incipient velocity. The median grain size of the prototype sediment of the dam body is 0.45 mm, and the incipient velocity ranges from 0.30 to 0.94 m s^{-1}. The similitude of velocity scale is 13.4, which means that the incipient velocity of the model sediment should range from 0.022 to 0.070 m s^{-1}. Sediment of different grain sizes was tested in flume experiments, and a model sediment with a median grain size of 0.12 mm and an incipient velocity ranging from 0.03 to 0.07 m s^{-1} was chosen. The major scales were obtained by the previous similarity equations, and are shown in Table 1.

Experimental Cases

This study focused on investigating the most unfavorable case of flood overtopping, for natural conditions (Case 1) and with artificial intervention for disaster mitigation (Case 2). The artificial intervention in Case 2 was aimed at delaying or preventing dam failure when overtopping occurs. In this case, coarse grains were added to the downstream face of the dam during the tailings accumulation. The grain size distribution of the coarse grains can be observed in Fig. 1. The coarse grains were 1.0 cm in diameter and were compacted during treatment preparation. The tailings mixed to some extent (0.5 cm thick) with the coarse grains, which simplified the building process and means that this can be done simultaneously with tailings deposition.

Table 1 Scales of Wadugou tailings impoundment model

Similarity conditions	Scales	Values
Geometric similarity	Horizontal scale	180
	Vertical scale	180
Similarity of water-flow	Velocity scale	13.4
	Discharge scale	434,692
	Time scale	13.4
	Roughness scale	2.38
	Grain size scale	4
Similarity of sediment movement	Grain density scale	1.25
	Dry grain density scale	2
	Incipient velocity scale	10.5–13.2
	Suspended load concentration scale	1.5
	Bed deformation time scale	17.9

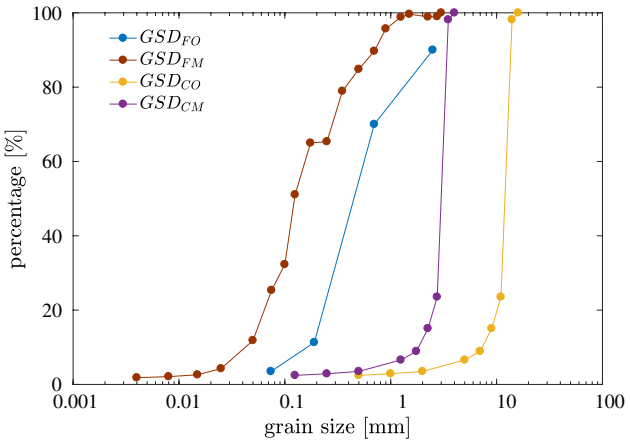

Fig. 1 Grain size distributions of sediment of the dam body. The GSD_{FO} and GSD_{FM} indicate the GSD of tailings sediment in the prototype and the model, respectively. The GSD_{CO} and GSD_{CM} correspond to the GSD of the coarse particles in Case 2 for the prototype and the model, respectively

Arrangement of the Physical Model

Four water-level monitoring points were set up during this experiment (Fig. 2). An automatic water-level tracker was used to monitor changes in downstream water levels after dam failure. Monitoring points #1 and #4 were located near the toe of the dam and the end of the model, respectively. Monitoring points #2 and #3 were distributed in the middle of the downstream trench. The monitoring points were 1.28, 3.22, 10.44, and 16.19 m downstream of the dam in the physical model, which corresponds to 230, 580, 1879, and 2915 m downstream in the prototype.

The topography model around the dam was made as a fixed model using bricks and cement and was built based on scaled elevation data. The downstream buildings were built following the geometric scale and placed in the physical model at their corresponding locations in the prototype. The model tailings were uniformly deposited in the dam reservoir. The Manning coefficient of the prototype downstream trench is 0.03–0.035, which means the Manning coefficient of the physical model should be 0.013–0.015, according to the resistance similitude. The small resistance coefficient required that the downstream model had a rather smooth surface, which was realized by polishing the cement surface. The compactness of the dam is an important factor that significantly affects the erodibility of the dam. Before running Cases 1 and 2, the dam body was compacted by an earth rammer using the same number of compactions. The bulk density of samples collected from different positions of the dam embankment was measured and the error was controlled within 2%, a value that has negligible influence on the experiments (Zhang et al. 2011).

The upstream boundary is an inflow condition and the flow inlet is set up in the upper reach at the left-side impoundment area. The flow discharge is a 200 year flood of 121.97 $m^3\ s^{-1}$ in the prototype, corresponding to 0.28 $L\ s^{-1}$ in the model. The flow was continued for 230 s for each case because the inflow volume in this time period is equivalent to the rainfall volume for the 200 year flood. The downstream boundary is an outflow boundary condition, which means the downstream model extends to a sufficient length

Fig. 2 Water level monitoring points and cross sections distribution

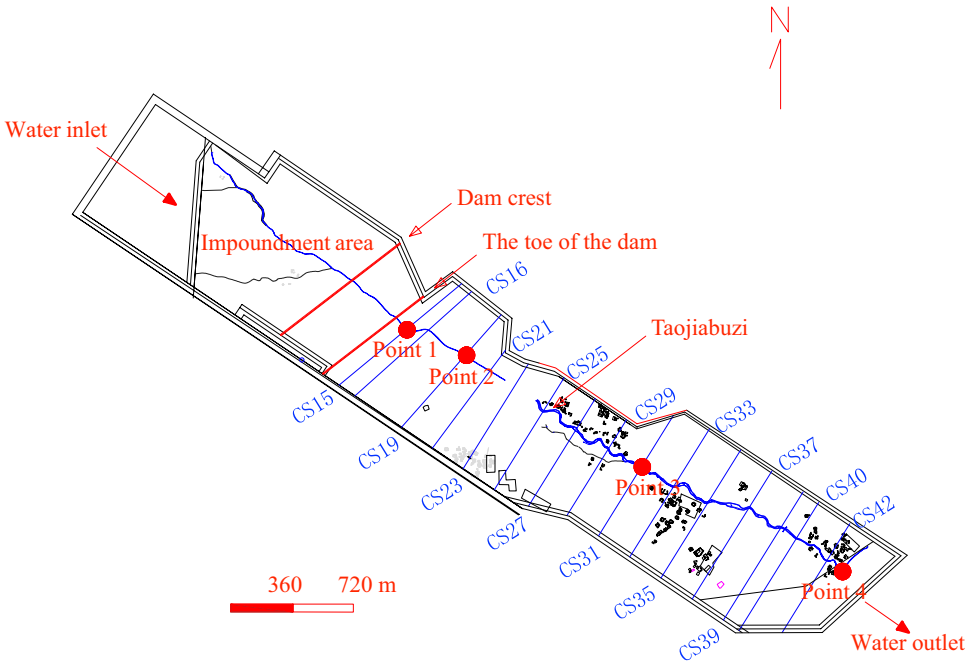

and the outflow has no impact on the upstream flow. Other than the upstream and downstream boundaries, there is no inflow or outflow through boundaries. The topography defined the fixed boundaries, and it is non-erodible during the experiment. The tailings dam and sediment in the reservoir can be eroded and the eroded sediment may deposit in the downstream channel.

Results

Experiment Observation

Figure 3a, b show how the water initially flows out from the dam crest. Figure 3c, d compares the downstream inundated areas 100 min after flood overtopping. It is evident that the inundated area of Case 1 is larger than that of Case 2. Figure 3e, f show the shapes and forms of the dam body after the test. Since no protective measure was adopted in Case 1, the water flow continuously scours and undercuts on the right of the dam body, and develops into a breach, in which tailings move as a mudflow. Since dam protective measures are taken in Case 2, no large breach occurs on the main body of the dam, though several rills occur at the dam crest. Tailings on the dam crest are washed away by the overtopping water flow. The scour depth is much smaller than in Case 1, and only a small amount of tailings flow out of the tailings impoundment.

Discharge Variations at the Dam Site

Figure 4 is the discharge curve at the toe of the dam during the process of dam failure; measurement begins when the overflow first occurs at the dam crest. Note that in Figs. 4 and 5, the parameter values are converted to prototype values based on the scales listed in Table 1. In Case 1, it takes about 16 min for the overflow at the dam crest to reach the toe of the dam. It reaches a peak value of 4812 $m^3\ s^{-1}$ at around 70 min, and it gradually decreases to less than 1000 $m^3\ s^{-1}$, 150 min later. During the rising and falling limbs, the flow

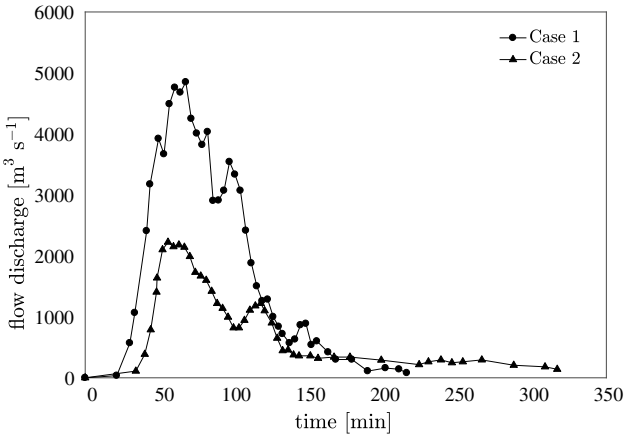

Fig. 4 Flow Discharge at the toe of the dam for Cases 1 and 2. The measurement of flow discharge begins when overflow occurs on the dam crest. Both the time and flow discharge are converted to prototype values

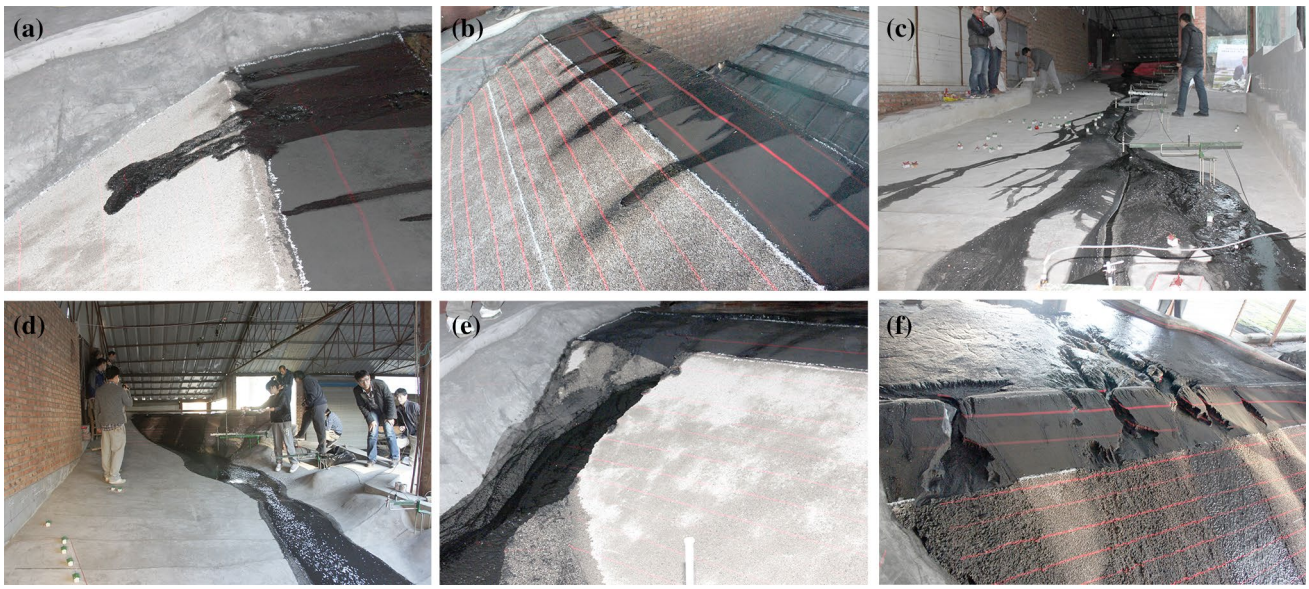

Fig. 3 Photos of the experiment. The overtopping phases of Case 1 and Case 2 are shown in **a** and **b**, respectively. **c, d** Show the downstream inundation areas after the overtopping (100 min later) for Case 1 and Case 2, respectively. The dam bodies of Case 1 and Case 2 at the end of the experiments are compared in **e** and **f**

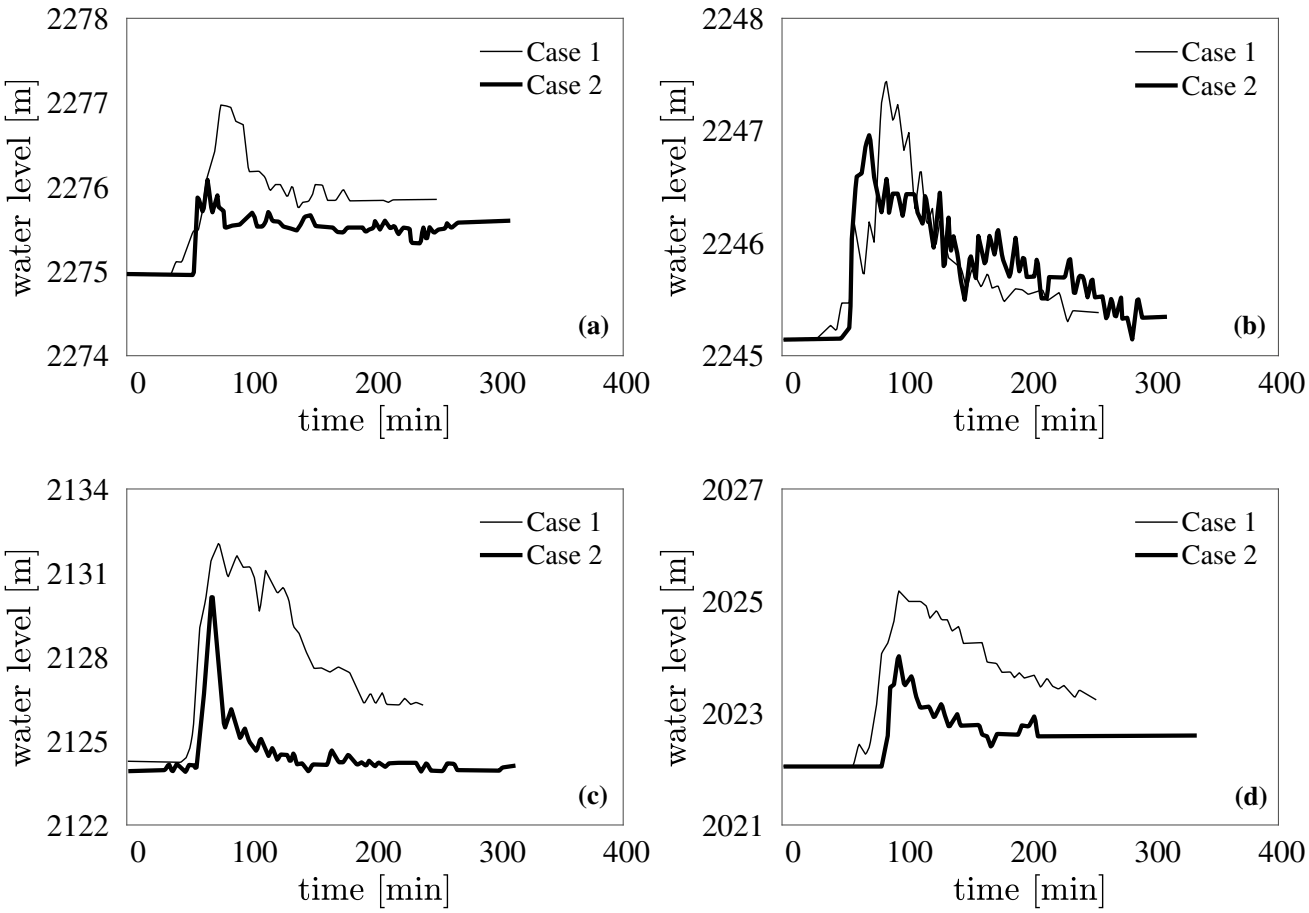

Fig. 5 Flood hydrograph at observation points, with plots **a, b, c**, and **d** correspond to monitoring points #1, #2, #3, and #4, respectively. The measurement of water level begins when overflow occurs on the dam crest. Both the time and water level are converted to prototype values

discharge does not constantly increase or decrease, though significant fluctuations are observed. The fluctuations are introduced by intermittent collapse of tailings in the breach, which also extends the flood peak. When artificial dam protective measures are adopted (Case 2), the dam body does not break, though several overflows occur at the dam crest. Because of the presence of the multiple overflow rills, flow converged quickly to the toe of the dam, and the flood peak in Case 2 occurs earlier than in Case 1. However, since the dam body was not destroyed in Case 2, the flow discharge varies over a limited range compared to Case 1 (the flood peak is 2224 $m^3 s^{-1}$, much less than in Case 1).

Flood Hydrograph of Downstream Trenches

Figure 5 shows the flood hydrograph at different monitoring points at the downstream trench. The water level is rather small at the initial stage of dam overtopping. At all monitoring points, the flood occurs later in Case 2 than Case 1. In Fig. 5a, the overtopped flow reaches monitoring point #1 at 33 min in Case 1, and at 54 min for Case 2. The time delays in Case 2 is 21, 12, and 28 min for monitoring points #2, #3, and #4, respectively. The shapes of the hydrographs are also different for the two cases. The rising limbs of the hydrograph in Case 2 are characterized by a rapid increase to the maximum water level, while the water levels gradually increase during the rising limbs in Case 1. The different hydrograph shapes are attributed to the overtopping flow process. In Case 1, the dam crest is gradually eroded into a large breach, and flow discharge, and thus water level, gradually increases during the breach-forming process. In contrast, multiple overflows emerge on the dam crest at almost the same time in Case 2, and no serious erosion occurs due to the protective measures. Consequently, the flow discharge and water level increase rapidly due to the convergence of flow, but with a much smaller discharge and water level. In addition, in Fig. 5c, d, the water level declines much slower in Case 1 than Case 2. This is due to the different amount of tailings deposited in the downstream trenches. Because the flow discharge is much greater in Case 1, tailing deposition is more serious, which keeps water levels at #3 and #4 high despite the continuously declining flow.

Mudflow Inundation Area

Figure 6 shows the downstream mudflow-inundated areas for both cases. In Case 1, the inundated area near the dam site is rather large, and the transverse width of the mudflow reaches 506 m at the CS19 cross-section. After that, the transverse width of the mudflow decreases downstream, reaching a minimum value of 101 m at the CS27 cross-section, near Taojiapuzi. It then increases again in the downstream direction. The large inundated area near the dam is caused by the tailings being transported from the dam crest and deposited at the toe of the dam where the bed slope suddenly decreases. Because of the increasing channel depth near Taojiapuzi, the transverse width of the mudflow decreases accordingly. Downstream of Taojiapuzi, the channel slope further decreases, which results in tailings deposition and thus an increased inundated area.

The inundated area of Case 2 is shown in Fig. 6b. The inundation trend of the central and downstream areas is similar to that of Case 1 in that it declines before increasing. However, a significant difference in the inundated area can be observed between Cases 1 and 2, due to the amount of tailings being transported by the flood. Because the flow discharge is much smaller in Case 2, less tailings are eroded and transported by the flow, which dramatically decreases tailings deposition downstream. In the prototype condition, the inundated area of Cases 1 and 2 are 0.91 and 0.50 km^2, respectively, which indicates that the protective measures reduced the impact by 0.41 km^2 or 45%.

Table 2 lists the highest flood level after dam failure for both cases. After overtopping, the flood rapidly moved toward the toe of the dam, and the potential energy of the water was converted into kinetic energy, introducing a very high flow velocity. After more than 500 m, most of the flood energy was dissipated, the water flow turned relatively smooth and steady, and the maximum water depth gradually declined. The flood level for Case 2 is significantly lower than in Case 1. In particular, within 1 km downstream of the dam body, most of the maximum flood depths were more than 50% less.

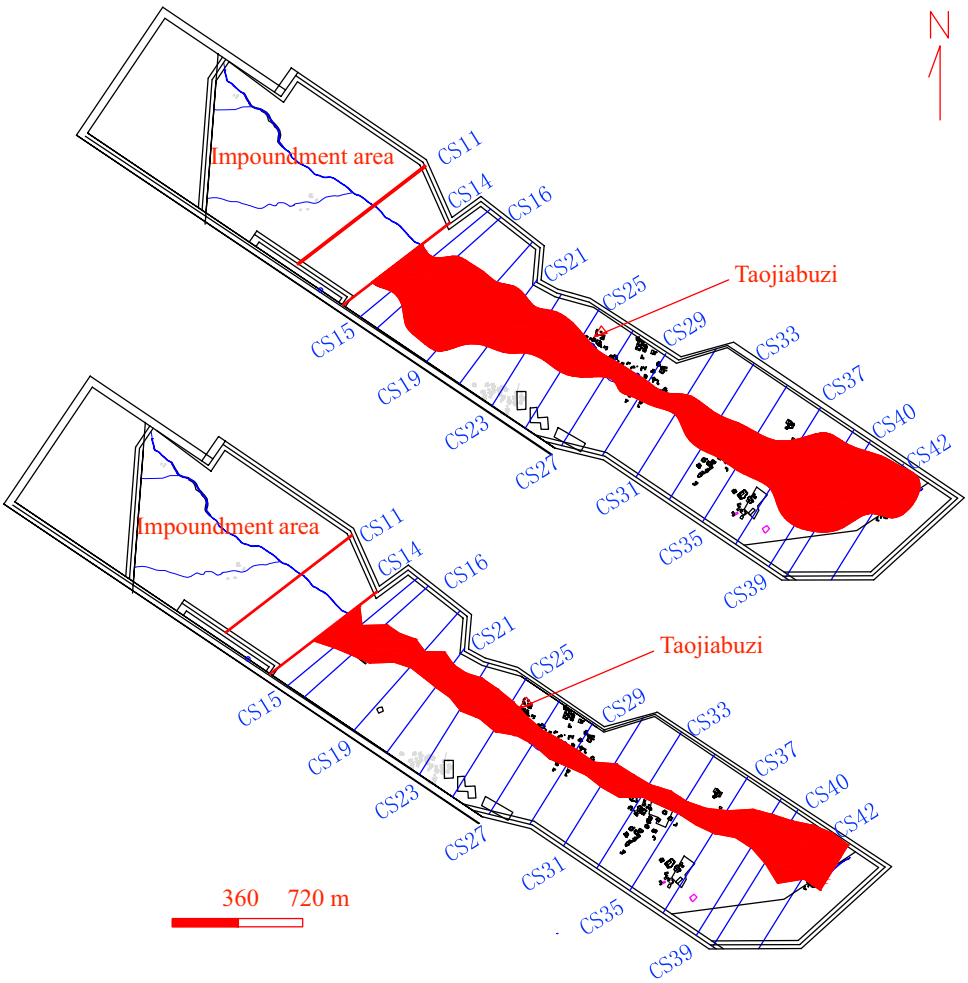

Fig. 6 The inundated area of model tests, with the upper and lower plots correspond to Case 1 and Case 2, respectively

Table 2 The highest flood levels of Case 1 and Case 2

Cross-sections	D	E_b	$L1_{max}$	$H1_{max}$	$L2_{max}$	$H2_{max}$	$H2_{max}/H1_{max}$
CS14	0.00	2284.00	2337.30	53.30	2318.40	34.40	0.64
CS15	89.54	2275.00	2311.56	36.56	2291.04	16.04	0.43
CS16	218.03	2263.00	2301.66	38.66	2280.96	17.96	0.46
CS19	475.52	2245.00	2273.64	28.64	2250.02	5.02	0.17
CS21	643.76	2228.00	2241.54	13.54	2231.10	3.10	0.22
CS23	809.49	2216.50	2220.80	4.30	2219.90	3.40	0.79
CS25	1034.96	2184.93	2198.00	13.07	2193.90	8.97	0.68
CS27	1286.70	2164.00	2172.42	8.42	2171.80	7.80	0.92
CS29	1537.08	2142.65	2155.74	13.09	2152.38	9.73	0.74
CS31	1770.56	2124.10	2135.08	10.98	2130.40	6.30	0.57
CS33	1986.59	2107.30	2119.67	12.37	2115.90	8.60	0.69
CS35	2225.06	2089.99	2098.64	8.65	2095.56	5.57	0.64
CS37	2461.83	2073.10	2080.74	7.64	2079.60	6.50	0.85
CS39	2695.87	2055.50	2065.24	9.74	2063.60	8.10	0.83
CS40	2804.60	2047.10	2056.50	9.40	2054.70	7.60	0.80
CS42	3030.03	2031.00	2039.22	8.22	2039.12	8.12	0.98

The cross-sections are labeled in Fig. 2. D is the downstream distance from the dam site (m); E_b is trench bottom elevation (m);$L1_{max}$ and $L2_{max}$ are the highest flood levels for Case 1 and Case 2 (m), respectively; $H1_{max}$ and $H2_{max}$ are the maximum inundation depths for Case 1 and Case 2 (m), respectively, with $H1_{max} = L1_{max} - E_b$ and $H2_{max} = L2_{max} - E_b$

Table 3 Comparison of the Case 1 and Case 2

Key parameters	Case 1	Case 2
The maximum breaching flow discharge ($m^3\ s^{-1}$)	4812	2224
The highest breaching flow velocity ($m\ s^{-1}$)	22.9	18.2
Total erosion volume (104 m^3)	179.1	86.6
Deposition volume in downstream trenches (104 m^3)	112.9	40.7
Duration of flood peaks (min)	39	28
Time for tailings to reach Taojiabuzi (min)	46.8	65.5

Discussion

Safe Evacuation Time

Table 3 summarizes key parameters from the test process. The parameters are significantly greater for Case 1 than for Case 2. In particular, the tailings erosion volume for Case 1 is nearly twice that of Case 2. Moreover, the flow velocity is greater for Case 1 while the time it takes for tailings to reach Taojiabuzi is better for Case 2. The comparison between the two cases confirms the validity of the protective measures. In addition, some more measures can also be adopted to extend the evacuation time during a tailings dam failure:

1. Building a flood release system. The system should be carefully examined each year before the flooding season to reduce the risk of a dam failure.
2. Establishing a connection with a local weather station to provide a rainfall forecast for the tailings reservoir area. In addition, an automatic rainfall gauge can be set up to provide more accurate measurements. When the 10 min rainfall intensity is above the design level, an emergency alert should be issued immediately.
3. Constructing a low dam downstream of the tailings dam. This low dam can effectively delay the movement of tailings and thus increase the evacuation time.
4. If it is possible, build an embankment around the village. The embankment should delay flooding in the village.

Significance of This Study

The key effect of the protective method adopted in Case 2 lies in stopping the overtopping flow from scouring the tailings from the downstream embankment, which significantly decreases the downgradient discharge and the amount of tailings transported by the flow, which in turn influences the consequence of the disaster. Since less tailings are deposited downstream, the water level at those locations are less affected. In addition, the reduced discharge makes the water level rise more slowly, which increases the evacuation time for downstream residents. In summary, the protective measures reduce the amount of transported tailings and the flooding discharge, which reduces the inundation area and detains the mudflow. Thus, the results of this study suggest that increasing the scouring resistance of the downstream embankment of a tailings dam reduces erosion, and thus lessens damage to the embankment. This reduces the impact

of a dam failure significantly. This suggests that this uncomplicated protective measure can and should be adopted at other tailings dams.

Conclusions

In this study, a physical model of the Wadugou tailings impoundment was built, based on water-flow and tailings sediment motion similitudes, to study the potential benefit of a new procedure on the process of overtopping during tailings dam failures. Its effect on delaying the dam-break process and disaster mitigation were analyzed. Based on the experimental results, some conclusions are:

1. The similarity conditions of tailings pond model test can be determined based on the model similarity law of a flood with a high sediment concentration;
2. The protective measures tested decreased the breach area, the maximum breaching flow discharge and flow velocity, the downstream inundated area, and the volume of eroded and deposited tailings during failure of a tailings dam by overtopping.
3. Without such protective measures, the time before substantial destruction occurs in a village downstream is much shorter. This study provides a valuable reference for the safe evacuation time in the emergency plan of the Wadugou tailings impoundment.

Acknowledgements Financial support from the National Key Research and Development Program (2016YFC0402506), the National Natural Science Foundation of China (51309084, 51509074), the Fundamental Research Funds for the Central Universities (2015B29114), and the Natural Science Foundation of Jiangsu Province (BK20140847) are gratefully acknowledged. We thank Prof. Zhang, Hongwu who helped us a lot during the revision process to improve the clarity and accuracy of the text.

References

Chanson H (1999) Physical modelling of hydraulics. In: Chanson H (ed) The hydraulics of open channel flow. Elsevier, London, pp 261–283

Costa JE, Schuster RL (1988) The formation and failure of natural dams. Geol Soc Am Bull 100(7):1054–1068

De Blasio FV, Elverhøi A, Issler D, Harbitz CB, Bryn P, Lien R (2004) Flow models of natural debris flows originating from overconsolidated clay materials. Mar Geol 213(1–4):439–455

Jeyapalan JK, Duncan JM, Seed HB (1983) Investigation of flow failures of tailings dams. J Geotech Eng 109(2):172–189

Korup O, Tweed F (2007) Ice, moraine, and landslide dams in mountainous terrain. Quat Sci Rev 26(25–28):3406–3422

Loukola E, Reiter P, Shen C, Pan S (1993) Embankment dams and their foundation: Evaluation of erosion. Proc, International Workshop on Dam Safety Evaluation, Grindewald, pp 171–188

Miller BGN, Cruden DM (2002) The Eureka river landslide and dam, Peace river Lowlands, Alberta. Can Geotech J 39(4):863–878

Nicoletti PG, Parise M (2002) Seven landslide dams of old seismic origin in southeastern Sicily (Italy). Geomorphology 46(3–4):203–222

Niekerk HJV, Viljoen MJ (2005) Causes and consequences of the Merriespruit and other tailings-dam failures. Land Degrad Dev 16(2):201–212

Pastor M, Fernández Merodo JA, Herreros MI, Mira P, González E, Haddad B, Quecedo M, Tonni L, Drempetic V (2007) Mathematical, constitutive and numerical modelling of catastrophic landslides and related phenomena. Rock Mech Rock Eng 41(1):85–132

Prime N, Dufour F, Darve F (2014) Solid–fluid transition modelling in geomaterials and application to a mudflow interacting with an obstacle. Int J Numer Anal Meth Geomech 38(13):1341–1361

Riba I, DelValls TA, Reynoldson TB, Milani D (2006) Sediment quality in Rio Guadiamar (SW, Spain) after a tailings dam collapse: contamination, toxicity and bioavailability. Environ Int 32(7):891–900

Rico M, Benito G, Díez-Herrero A (2008) Floods from tailings dam failures. J Hazard Mater 154(1–3):79–87

Sammarco O (2004) A tragic disaster caused by the failure of tailings dams leads to the formation of the Stava 1985 foundation. Mine Water Environ 23(2):91–95

Simpson G, Castelltort S (2006) Coupled model of surface water flow, sediment transport and morphological evolution. Comput Geosci 32(10):1600–1614

Sun E, Zhang X, Li Z, Wang Y (2012) Tailings dam flood overtopping failure evolution pattern. Proced Eng 28:356–362

Tabri K, Määttänen J, Ranta J (2008) Model-scale experiments of symmetric ship collisions. JMST 13(1):71–84

Wang T, Zhou Y, Lv Q, Zhu Y, Jiang C (2011) A safety assessment of the new Xiangyun phosphogypsum tailings pond. Miner Eng 24(10):1084–1090

Yin G, Wei Z, Wang JG, Wan L, Shen L (2008) Interaction characteristics of geosynthetics with fine tailings in pullout test. Geosynth Int 15(6):428–436

Yin G, Li G, Wei Z, Wan L, Shui G, Jing X (2011) Stability analysis of a copper tailings dam via laboratory model tests: a Chinese case study. Miner Eng 24(2):122–130

Zandarín MT, Oldecop LA, Rodríguez R, Zabala F (2009) The role of capillary water in the stability of tailings dams. Eng Geol 105(1–2):108–118

Zhang Y, Li X, Wu T, Hong J (2007) Study on scale calculation of sediment concentration of suspended-load mobile-bed model testing. Yellow River 29(12):33–35 **(Chinese)**

Zhang H, Liu L, Bu H, Zhong D (2011) Test and design of tailings dam model. Yellow River 33(12):1–5 **(Chinese)**

Zhao Y, Zhou X, Jing X. Liu K, Ye C, Zhang X (2015) Experimental study on overtopping failure mode of reinforced tailing dam. In: Proc, 3rd international conf on advances in energy and environmental science, Zhuhai, pp 1414–1419